Open quantum dynamics of strongly coupled oscillators with multi-configuration time-dependent Hartree propagation and Markovian quantum jumps

(iD) Johan F. Triana and (iD) Felipe Herrera

COLLECTIONS

View Online   **Export Citation**   **CrossMark**

ARTICLES YOU MAY BE INTERESTED IN

Open quantum dynamics of strongly coupled oscillators with multi-configuration time-dependent Hartree propagation and Markovian quantum jumps

View Online   Export Citation   CrossMark

Johan F. Triana[1] (iD) and Felipe Herrera[1,2,a)] (iD)

AFFILIATIONS

[1] Department of Physics, Universidad de Santiago de Chile, Av. Victor Jara, 3493 Santiago, Chile
[2] ANID-Millennium Institute for Research in Optics, Concepción, Chile

Note: This paper is part of the 2022 JCP Emerging Investigators Special Collection.
[a)]Author to whom correspondence should be addressed: felipe.herrera.u@usach.cl

ABSTRACT

Modeling the non-equilibrium dissipative dynamics of strongly interacting quantized degrees of freedom is a fundamental problem in several branches of physics and chemistry. We implement a quantum state trajectory scheme for solving Lindblad quantum master equations that describe coherent and dissipative processes for a set of strongly coupled quantized oscillators. The scheme involves a sequence of stochastic quantum jumps with transition probabilities determined by the system state and the system-reservoir dynamics. Between consecutive jumps, the wave function is propagated in a coordinate space using the multi-configuration time-dependent Hartree method. We compare this hybrid propagation methodology with exact Liouville space solutions for physical systems of interest in cavity quantum electrodynamics, demonstrating accurate results for experimentally relevant observables using a tractable number of quantum trajectories. We show the potential for solving the dissipative dynamics of finite size arrays of strongly interacting quantized oscillators with high excitation densities, a scenario that is challenging for conventional density matrix propagators due to the large dimensionality of the underlying Hilbert space.

I. INTRODUCTION

Accurate numerical simulations of open quantum systems are fundamentally important for the development of quantum technology.[1] Understanding and possibly controlling system-reservoir interactions enables a diverse set of applications such as the manipulation of quantum speed limits for driven state evolution,[2] quantum metrology with improved precision bounds,[3,4] quantum circuits with improved gate fidelities,[5] quantum optics with nanophotonics,[6,7] or controlled chemistry with quantum optics.[8,9] In many applications, the temporal correlations of the reservoir variables that couple with the system of interest decay much faster than the system-reservoir interaction times. The open quantum system dynamics can then be modeled with Markovian quantum master equations for the evolution of the reduced system density matrix $\hat{\rho}_S$.[10,11] For a Hilbert space of dimension d, the density matrix scales with d^2, making the direct integration of quantum master equations numerically intractable for large many-body problems, as d scales exponentially with the number of particles.[12]

To simulate the dynamics of open quantum many-body systems, several techniques have been developed, including stochastic methods,[13,14] semi-classical methods,[15] tensor network representations,[16–18] phase space methods,[19–21] variational methods,[22] cluster expansions,[23–25] and field theory techniques.[26–28] Broadly speaking, these approaches differ in the way the density matrix and quantum master equation are represented and propagated. Advanced simulation techniques are commonly used in chemical physics for treating strong molecules in complex reservoirs.[29–32] Cavity quantum electrodynamics (QED) with molecules has emerged as another domain in which advanced

quantum dynamics methods are useful,[9,33–35] as the emergence of cavity-induced single-particle and many-body correlations is believed to be relevant for explaining experiments on the modification of chemical reaction rates in optical and infrared cavities.[8,31,36–44]

We develop a stochastic wave function methodology for solving Markovian quantum master equations in the coordinate representation. The stochastic component of the method is based on the Dalibard–Castin–Molmer quantum jump technique,[14] a type of Monte Carlo method[45] where the system wave function undergoes a sequence of quantum jumps with transition probabilities determined by the instantaneous state of the system and the physics of the system-reservoir coupling. Between consecutive quantum jumps, the wave function evolves deterministically according to the instantaneous Hamiltonian, which we represent in a coordinate space using the multi-configuration time-dependent Hartree (MCTDH) method.[46,47] Observables in the quantum jump technique are guaranteed to converge to the density matrix solution of the quantum master equation by averaging over a sufficient number of wave function trajectories.[14] The scheme is applicable to Markovian master equations in Lindblad form,[11] but extensions to more general reservoirs have been developed.[48,49]

Wave function trajectories in the coordinate representation are particularly well suited for studying strongly interacting oscillators subject to driving and dissipation, as often found in molecular cavity QED problems.[9,33,34] The system wave function can be propagated in a coordinate space for any suitable light–matter interaction gauge.[50,51] MCTDH propagators can already capture strong correlations between high-dimensional anharmonic oscillators that naturally emerge in chemical physics.[52–56] Therefore, extending the MCTDH method beyond the use of complex potentials[42,57] is a significant step toward scalable atomistic modeling of many-body molecular cavity QED systems. Recently, an equivalent combination of the Monte Carlo wave function method with the MCTDH has been implemented in Refs. 58 and 59 for a vibrational energy transfer problem.[60]

In what follows, we briefly review the quantum jump and MCTDH methods (Sec. II). Then, we demonstrate the applicability of the proposed methodology and explore its limitations (Sec. III) and suggest possible applications of the method for studying cavity QED with molecular oscillators (Sec. IV).

II. METHODS

A. Monte Carlo wave function method

For Markovian open quantum systems,[10,61] the evolution of the density matrix $\hat{\rho}_S$ in Liouville space is determined by a quantum master equation, which in Lindblad form reads ($\hbar \equiv 1$ is used throughout)[11]

$$\frac{d}{dt}\hat{\rho}_S(t) = i[\hat{H}_S, \hat{\rho}_S(t)] + \sum_j \hat{L}_j \hat{\rho}_S(t)\hat{L}_j^\dagger - \frac{1}{2}\{\hat{L}_j^\dagger \hat{L}_j, \hat{\rho}_S(t)\}, \quad (1)$$

where $\hat{H}_S$ is the system Hamiltonian and $\hat{L}_j$ are Lindblad jump operators that describe the interaction between the system and the jth reservoir channel. The square brackets denote the commutator, and the curly brackets, the anticommutator. The Lindblad form of the master equation is a dynamical semi-group that ensures the

positivity of the density matrix.[11] The Monte Carlo wave function technique avoids the direct integration of the quantum master equation by propagating an initial wave function $\Psi(0)$ over a sequence of non-Hermitian evolution intervals that are interrupted at random times by quantum jumps that encode the physics of the Lindblad operators $\hat{L}_j$.[14]

Figure 1 summarizes the proposed Monte Carlo-MCTDH (MC-MCTDH) algorithm. Starting from a reference time t, the wave function $|\Psi(t)\rangle$ is propagated with the MCTDH method up to $t + \Delta t$ with the effective non-Hermitian Hamiltonian

$$\hat{H} = \hat{H}_S - \frac{i}{2}\sum_j \hat{L}_j^\dagger \hat{L}_j. \quad (2)$$

For small Δt, the wave function norm is reduced as

$$\langle \Psi(t+\Delta t)|\Psi(t+\Delta t)\rangle = 1 - \delta p, \quad (3)$$

where $\delta p = \sum_j \delta p_j$ is determined by the instantaneous jump probabilities $\delta p_j = \Delta t \langle \Psi(t)|\hat{L}_j^\dagger \hat{L}_j|\Psi(t)\rangle$. At the end of the interval, a pseudo-random number $0 < \epsilon < 1$ is generated from a uniform distribution and compared with δp. If $\delta p \le \epsilon$, no quantum jump occurs and the wave function is renormalized as

$$|\Psi'(t+\Delta t)\rangle = \frac{|\Psi(t+\Delta t)\rangle}{\sqrt{1-\delta p}}, \quad (4)$$

before another interval begins. If $\delta p > \epsilon$, a quantum jump occurs and a Lindblad jump operator is chosen to act on the wave function. The jth reservoir channel is chosen such that the operator $\hat{L}_j$ gives the
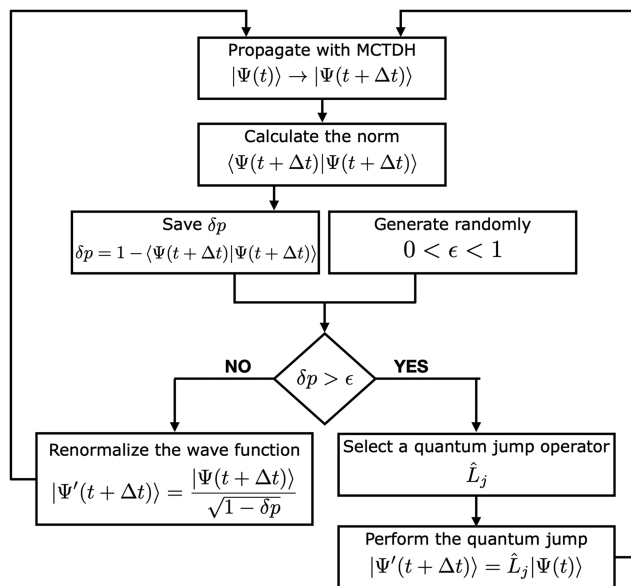

FIG. 1. Flowchart of the MC-MCTDH algorithm. Deterministic propagation steps with multi-configuration time-dependent Hartree (MCTDH) steps with stochastic quantum jumps on the wave function due to system-reservoir coupling.

smallest jump probability δ_j that is greater than ϵ. The new wave function after the jump becomes

$$|\Psi'(t+\Delta t)\rangle = \frac{\hat{L}_j|\Psi(t)\rangle}{\sqrt{\delta p_j/\Delta t}}, \tag{5}$$

and a new interval begins. The steps are sequentially repeated until the propagation ends, resulting in a piecewise quantum trajectory for the system wave function.

Observables are computed by averaging instantaneous expectation values over multiple trajectories.[14] For the kth quantum trajectory, expectation values $\langle\Psi^{(k)}(t)|\hat{O}|\Psi^{(k)}(t)\rangle$ are computed at the end of each interval, after normalizing the wave function. The procedure is straightforward to extend for computing two-time correlation functions.[10] By construction, any trajectory-averaged observable

$$\overline{\langle\hat{O}(t)\rangle} = \frac{1}{n_T}\sum_{k=1}^{n_T}\langle\Psi^{(k)}(t)|\hat{O}|\Psi^{(k)}(t)\rangle \tag{6}$$

asymptotically converges to the density matrix solution $\langle\hat{O}\rangle \equiv \text{Tr}[\hat{\rho}_S(t)\hat{O}]$ with the increasing number of trajectories n_T. The convergence proof can be found in Ref. 14 and is reproduced in the Appendix. In practice, quantum optics problems allow for $n_T \sim 10^2$. Mean-squared errors (MSE) of the average observables can be defined by comparing with the exact density matrix solutions (see the Appendix). The independence of each trajectory facilitates computational parallelization strategies.

B. MCTDH propagator

We use the MCTDH method for the deterministic propagation step in Fig. 1. The method was developed by Meyer, Manthe, and Cederbaum in 1990[46] as a generalization of the time-dependent Hartree ansatz[62] for solving the time-dependent Schrödinger equation. The MCTDH is widely used in chemical physics due to its ability to obtain essentially exact fully quantum results for complex molecular systems with a large number of vibrational modes and strong non-adiabatic interactions.[63,64]

The standard ansatz for solving the time-dependent Schrödinger equation is an expansion in a time-independent basis with time-dependent coefficients of the form

$$\Psi(q_1,\ldots,q_f,t) = \sum_{j_1=1}^{N_1}\ldots\sum_{j_f=1}^{N_f} C_{j_1\ldots j_f}(t)\prod_{k=1}^{f}\chi_{j_k}^{(k)}(q_k), \tag{7}$$

where q_k are system coordinates, $C_{j_1\ldots j_f}(t)$ are dynamical expansion coefficients, and $\chi_{j_k}^{(k)}$ are the time-independent basis functions that describe the kth degree of freedom. For example, in molecular vibration problems, there would be f degrees of freedom (e.g., vibrational modes) in this expansion, each described by a complete basis of N_{j_k} basis functions (e.g., vibrational eigenfunctions) represented on a one-dimensional coordinate grid using discrete variable representation (DVR) techniques.[65]

The MCTDH method generalizes the static product basis in Eq. (7) with a linear combination of time-dependent Hartree products of the form

$$\Psi(q_1,\ldots,q_f,t) = \sum_{j_1=1}^{n_1}\ldots\sum_{j_f=1}^{n_f} A_{j_1\ldots j_f}(t)\prod_{k=1}^{f}\phi_{j_k}^{(k)}(q_k,t)$$
$$= \sum_J \mathbf{A}_J(t)\mathbf{\Phi}_J(t), \tag{8}$$

where the collective index J labels the set of basis functions ϕ_{j_k} in a given tensor product configuration that contributes to the wave function, the tensor $\mathbf{A}_J(t) \equiv A_{j_1\ldots j_f}(t)$ contains the time-dependent amplitudes of each product configuration, and $\mathbf{\Phi}_J(t) \equiv \prod_{k=1}^{f}\phi_{j_k}^{(k)}(q_k,t)$ denotes the instantaneous product basis configurations. The number of relevant basis states per configuration and degree of freedom n_k in Eq. (8) is typically smaller than the number of DVR basis functions N_k needed for convergence to the static ansatz in Eq. (7). As a result of this dynamical Hilbert space contraction, the number of product configurations $n_1 \times n_2 \times \cdots \times n_f$ needed for convergence is usually smaller than the number of static configurations in the standard method because $n_k < N_k$ for each kth degree of freedom, which becomes important when solving high-dimensional quantum dynamics problems.

The time-dependent Schrödinger equation is solved with the MCTDH ansatz [Eq. (8)] and the Dirac–Frenkel variational principle.[64] Coupled non-linear equations for the $\mathbf{A}_J$ and $\mathbf{\Phi}_J$ tensors are usually derived by introducing projectors over individual degrees of freedom $\hat{P}^{(k)} \equiv \sum_{j=1}^{n_k}|\phi_j^{(k)}\rangle\langle\phi_j^{(k)}|$, which are complete in the limit $n_k \to \infty$. Projecting Eq. (8) over the kth degree of freedom gives

$$\hat{P}^{(k)}\mathbf{\Psi} = \sum_{l=1}^{n_k}|\phi_l^{(k)}\rangle\langle\phi_l^{(k)}|\mathbf{\Psi}\rangle_k = \sum_{l=1}^{n_k}\phi_l^{(k)}\mathbf{\Psi}_l^{(k)}, \tag{9}$$

which, for the $k = 1$ degree-of-freedom, for example, would give an expansion in the complementary space of the form $\mathbf{\Psi}_l^{(1)} = \sum_{j_2}^{n_2}\cdots\sum_{j_f}^{n_f} A_{lj_2\ldots j_f}(t)\phi_{j_2}^{(2)}\cdots\phi_{j_f}^{(f)}$. Variations of the time-dependent coefficients $\mathbf{A}_J$ and one-dimensional time-dependent functions $\mathbf{\Phi}_J$ are given by

$$\frac{\delta\Psi}{\delta\mathbf{A}_J} = \mathbf{\Phi}_J, \tag{10}$$

$$\frac{\delta\Psi}{\delta\phi_{j_k}^{(k)}} = \mathbf{\Psi}_{j_k}^{(k)}, \tag{11}$$

$$\dot{\mathbf{\Psi}} = \sum_J \dot{\mathbf{A}}_J\mathbf{\Phi}_J + \sum_{k=1}^{f}\sum_{j_k=1}^{n_k}\dot{\phi}_{j_k}^{(k)}\mathbf{\Psi}_{j_k}^{(k)}. \tag{12}$$

Equations of motion for tensor coefficients $\mathbf{A}(t)$ are derived using Eqs. (8), (10), and (12) in the Dirac–Frenkel variational principle $\langle\delta\Psi|\hat{H}|\Psi\rangle = i\langle\delta\Psi|\frac{\partial}{\partial t}|\Psi\rangle$ to get the set of coupled non-linear equations

$$\sum_L \mathbf{A}_L\langle\mathbf{\Phi}_J|\hat{H}|\mathbf{\Phi}_L\rangle = i\sum_L \dot{\mathbf{A}}_L\langle\mathbf{\Phi}_J|\mathbf{\Phi}_L\rangle + i\sum_{k=1}^{f}\sum_{l=1}^{n_k}\langle\mathbf{\Phi}_J|\dot{\phi}_l^{(k)}\mathbf{\Phi}_L\rangle \tag{13}$$

and

$$i\dot{\mathbf{A}}_J = \sum_L \mathbf{A}_L\langle\mathbf{\Phi}_J|\hat{H}|\mathbf{\Phi}_L\rangle - i\sum_{k=1}^{f}\sum_{l=1}^{n_k}\mathbf{A}_{J_l^k}g_{jl}^{(k)} \tag{14}$$

with the constraint $g_{jl}^{(k)} = i\langle\phi_j^{(k)}|\dot{\phi}_l^{(k)}\rangle = i\langle\phi_j^{(k)}|\hat{g}^{(k)}|\phi_l^{(k)}\rangle$. In Eq. (14), the tensor elements per degree of freedom are denoted as $\mathbf{A}_{J_l^k} \equiv A_{j_1...l...j_f}$.

The equations of motion for the functions $\phi_{j_k}^{(k)}$ are also found variationally from the time-dependent Schrödinger equation. In terms of the projection operators $\hat{P}^{(k)}$, they read

$$\sum_{l_k}\langle\hat{H}\rangle_{j_k l_k}^{(k)}\phi_{l_k}^{(k)} = P^{(k)}\sum_{l_k}\langle\hat{H}\rangle_{j_k l_k}^{(k)}\phi_{l_k}^{(k)} + i\sum_{l_k}\rho_{j_k l_k}^{(k)}\dot{\phi}_{l_k}^{(k)}, \quad (15)$$

$$i\dot{\phi}_{j_k}^{(k)} = \sum_{l_k,m_k}\left(\boldsymbol{\rho}^{(k)^{-1}}\right)_{j_k l_k}\left(1 - P^{(k)}\right)\langle\hat{H}\rangle_{l_k m_k}^{(k)}\phi_{m_k}^{(k)}, \quad (16)$$

where $\rho_{j_k l_k}^{(k)} \equiv \langle\boldsymbol{\Psi}_{j_k}^{(k)}|\boldsymbol{\Psi}_{l_k}^{(k)}\rangle$ is a reduced density matrix and $\langle\hat{H}\rangle_{jl}^{(k)} = \langle\boldsymbol{\Psi}_j^{(k)}|\hat{H}|\boldsymbol{\Psi}_l^{(k)}\rangle$ is the mean-field Hamiltonian of the kth degree of freedom. The solution to the MCTDH equations of motion preserves the norm and total energy for time-independent Hermitian Hamiltonians. In this work, we use an extension of the method that includes non-Hermitian (complex) potentials. The complex character of the Hamiltonian is not treated as a complex absorbing potential in the MCTDH Heidelberg package. We coded the Hamiltonian directly on the integration routines of the package. Additional details about the MCTDH method can be found in Refs. 46, 64, and 66.

III. RESULTS

We test the proposed MC-MCTDH method by solving selected open quantum system problems of interest in cavity QED. For comparison, we also solve the corresponding Lindblad quantum master equation for the density matrix using the open source Python library QuTiP.[67] The same desktop machine is used for all calculations (3.0 GHz Intel Core i5 CPU, 8 GB RAM), unless otherwise stated.

A. Cavity field with finite photon lifetime

Consider a cavity mode with resonance frequency ω_c in a structure with imperfect mirror reflectivity. The mode is modeled as a quantum harmonic oscillator with annihilation operator $\hat{a}$. Cavity photons leak out to the far field at rate κ. A minimal decoherence model for radiative decay can be constructed with the Lindblad operator $\hat{L}_\kappa = \sqrt{\kappa}\,\hat{a}$. The effective Hamiltonian for the deterministic steps of the Monte Carlo propagation method is, thus, given by

$$\hat{H} = (\omega_c - i\kappa/2)\,\hat{a}^\dagger\hat{a}. \quad (17)$$

The Heisenberg equation of motion for the number operator $\hat{n} = \hat{a}^\dagger\hat{a}$ has the simple solution $\langle\hat{n}(t)\rangle = \langle\hat{n}(0)\rangle\exp[-\kappa t]$, i.e., exponential decay of initial occupation number $\langle\hat{n}(0)\rangle$ with population decay time $T_1 = 1/\kappa$. In Fig. 2, we show the MC-MCTDH evolution of an initial Fock state with $\langle\hat{n}(0)\rangle = 8$ photons, together with the analytical solution. The inset shows that a MSE ≈ 1% can be achieved with about $n_T = 400$ quantum trajectories.

This one-dimensional example is not exploiting the MCTDH tensor ansatz, but demonstrates the stochastic quantum jumps on a DVR grid for an excited Fock state. In general, most photonic states of interest in quantum optics (Fock state, coherent states, and squeezed light) can be accurately represented with DVR grids,[68] which could be advantageous in comparison with more elaborate phase-space representations.[15,69]
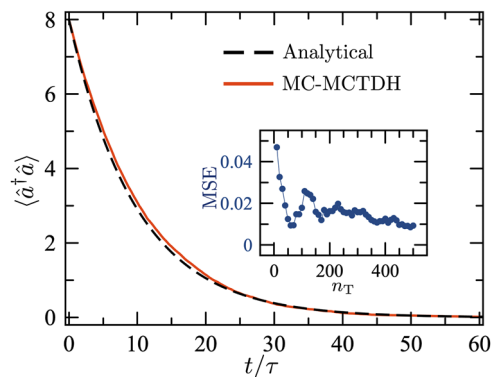

FIG. 2. Exponential decay of a lossy cavity. Simulated decay of an $n = 8$ Fock state with $n_T = 200$ MC-MCTDH quantum trajectories (solid line). The analytical solution is shown for comparison (dashed line). Time is in units of the cavity oscillation period $\tau = 2\pi/\omega_c$, and $\kappa = 0.016\omega_c$ is the photon decay rate. Inset: Mean-squared error (MSE) as a function of the number of trajectories.

B. Vacuum Rabi oscillations

Our next case study is two bilinearly coupled quantum harmonic oscillators in the rotating wave approximation. For an initial state with a single excitation in one of the oscillators, i.e., $|\Psi(0)\rangle = |1\rangle|0\rangle$, we expect the MC-MCTDH algorithm to describe damped Rabi oscillations of the subsystem variables. For a harmonic oscillator with annihilation operator $\hat{b}$ and resonance frequency ω_0 (e.g., molecular vibration) interacting with a cavity field $\hat{a}$ of frequency ω_c, the effective Hamiltonian is given by

$$\hat{H} = (\omega_c - i\kappa/2)\hat{a}^\dagger\hat{a} + (\omega_0 - i\gamma/2)\hat{b}^\dagger\hat{b} + g(\hat{b}^\dagger\hat{a} + \hat{b}\hat{a}^\dagger), \quad (18)$$

where g is the coupling strength (Rabi frequency). The dissipation of the b-oscillator at rate γ is modeled with the Lindblad operator $\hat{L}_\gamma = \sqrt{\gamma}\,\hat{b}$, and cavity dissipation is described as before.

Figure 3 shows the evolution of the occupation number $\langle\hat{b}^\dagger\hat{b}\rangle$ obtained with the MC-MCTDH method for a strong resonant coupling ($\omega_c = \omega_0$ and $g/\omega_c > 0.1$). The exact density matrix solution is also shown for comparison. For the chosen system parameters, averaging over $n_T = 50$ quantum trajectories gives a good short-time accuracy, although errors tend to accumulate at longer times ($t > 20 \times 2\pi/\omega_c$). Increasing the number of trajectories ($n_T \sim 200$) gives results that better match the exact Liouville-space solution.

C. Jaynes–Cummings revivals in driven cavities

We now study the coupling of a two-level atom (qubit) with a cavity field $\hat{a}$ prepared in a coherent state $|\alpha\rangle$ with (real) amplitude α. In the number (Fock) basis, the coherent state gives a Poissonian distribution with $\langle\hat{a}^\dagger\hat{a}\rangle = |\alpha|^2$.[61] Unitary dynamics is governed by the Jaynes–Cummings Hamiltonian[70,71]

$$\hat{H}_0 = \frac{1}{2}\omega_0\hat{\sigma}_z + \omega_c\hat{a}^\dagger\hat{a} + g(\hat{\sigma}_+\hat{a} + \hat{\sigma}_-\hat{a}^\dagger), \quad (19)$$

where $\hat{\sigma}_z$ and $\hat{\sigma}_\pm$ are the Pauli spin-1/2 operators, ω_0 is the qubit frequency, and g is the Rabi frequency. Since the spins do not
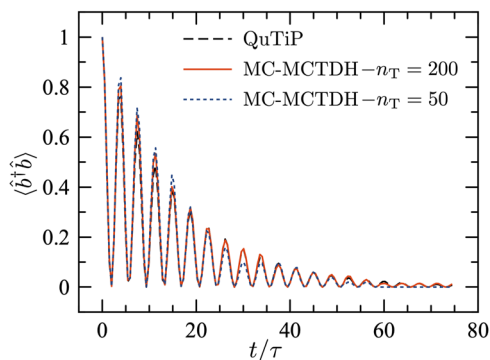
FIG. 3. Vacuum Rabi oscillations. Coherent transfer of a single initial excitation between two resonantly coupled harmonic oscillators, obtained with the MC-MCTDH for two sets of quantum trajectories $n_T = (50, 200)$. The QuTiP Liouville space solution is shown for comparison (black dashed line). The frequency of the b-oscillators is ω_0, the dissipation rates are $\kappa = 0.026\omega_0$ and $\gamma = 0.013\omega_0$, and the bilinear coupling strength is $g = 0.13\omega_0$. Time in units of $\tau \equiv 2\pi/\omega_0$.

have a coordinate dependence, we represent the two spin projections $m_z = \pm 1/2$ in a DVR grid using two flat potentials separated in energy by ω_0, i.e., $V_\pm(q) = \pm\omega_0/2$. This is equivalent to having two electronic states in the MCTDH package.[47] Pauli operators can be constructed accordingly. Atomic relaxation at the rate γ is given by the Lindblad operator $\hat{L}_\gamma = \sqrt{\gamma}\hat{\sigma}_-$, and cavity decay is described before. The effective Hamiltonian for deterministic propagation is given by $\hat{H} = \hat{H}_0 - i(\kappa/2)\,\hat{a}^\dagger\hat{a} - i(\gamma/2)\,\hat{\sigma}_+\hat{\sigma}_-$, with $\hat{H}_0$ in Eq. (19).

Figure 4 shows the evolution of the inversion $W(t) = \rho_{ee}(t) - \rho_{gg}(t)$, where ρ_{ii} denotes level population. The qubit is initialized in the excited level ($W(0) = 1$) and strongly couples to a cavity that has initially $|\alpha|^2 = 5$ photons on average. The Rabi frequency is $g = 0.13\omega_0$. For the small damping rates used ($\kappa = \gamma \sim 10^{-3}\omega_0$), the MC-MCTDH method reproduces the long-time revivals of
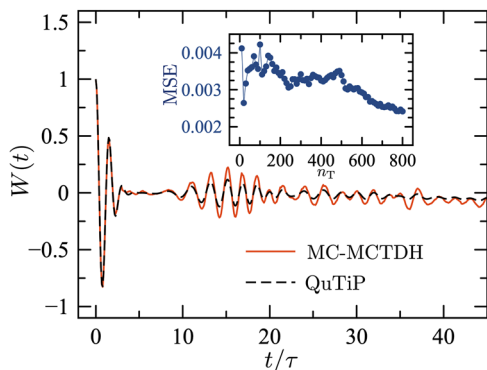

FIG. 4. Jaynes–Cummings population revivals in a driven cavity. MC-MCTDH evolution of the atomic inversion $W(t)$ for a qubit in a cavity initially prepared in a coherent state with $|\alpha| = 5$ average photons, for $n_T = 400$ quantum trajectories (solid red line). The Liouville-space solution is shown for comparison (dashed black line). Inset: Mean squared error (MSE) as a function of the number of trajectories. The qubit frequency is ω_0, the dissipation rates are $\kappa = \gamma = 3.5 \times 10^{-3}\omega_0$, and the Rabi frequency is $g = 0.13\omega_0$. Time in units of $\tau = 2\pi/\omega_0$.

the population inversion expected due to the exchange of coherence between qubit and Fock sub-levels that compose the coherent state,[71] using only $n_T = 400$ quantum trajectories. Deviations from the exact Liouville-space solution are negligible at short times, but grow over longer timescales. The inset in Fig. 4 shows the drop of the MSE with the increasing number of trajectories.

D. Independent quantum oscillators coupled to a common cavity field

In this example, we consider a set of N independent oscillators $\hat{b}_i$ that couple with a common quantized cavity field $\hat{a}$. The non-Hermitian effective Hamiltonian of the system is given by

$$\hat{H} = \omega_c\hat{a}^\dagger\hat{a} - \frac{i\kappa}{2}\hat{a}^\dagger\hat{a} + \sum_{i=1}^{N}\left[\omega_0\hat{b}_i^\dagger\hat{b}_i + g(\hat{b}_i^\dagger\hat{a} + \hat{b}_i\hat{a}^\dagger) - \frac{i\gamma}{2}\hat{b}_i^\dagger\hat{b}_i\right], \quad (20)$$

with jump operators for the b-oscillators $\hat{L}_{i\gamma} = \sqrt{\gamma}\hat{b}_i$, and cavity dissipation described as before. We focus on the coherent population transfer between oscillators beyond the single-excitation manifold.

Figure 5(a) shows the MC-MCTDH evolution of the occupation numbers $\langle\hat{b}_1^\dagger\hat{b}_1\rangle$ and $\langle\hat{b}_3^\dagger\hat{b}_3\rangle$ for a set of $N = 4$ oscillators in a cavity that initially has one excitation in b_1 and another excitation in b_2, with the cavity field in the vacuum, i.e., $|\Psi(0)\rangle = |1, 1, 0, 0, n = 0\rangle$. The results converge to the exact Liouville-space solution for the b-variables for $n_T = 200$ quantum trajectories. However, Fig. 5(b) shows that long-time errors of about 4% tend to accumulate for the photon number $\langle\hat{a}^\dagger\hat{a}\rangle$ after several population transfer cycles, which could be reduced by increasing n_T. The inset in Fig. 5(b) shows that the method captures the short-time rise and long-time decay of the $n = 2$ Fock state population P_2. Since the amount of ground state bleaching is significant (>10%), the Hilbert space dimension needed to converge to the Liouville-space solution is higher than that for the previous examples. For the parameters in Fig. 5, QuTiP solutions converge with a minimum Hilbert space dimension of $d \equiv (\nu_{max} + 1)^N \times (n_{max} + 1) = 324$, where $\nu_{max} = 2$ is the maximum quantum number used for each of the b-oscillators and $n_{max} = 3$ is the highest Fock state included.

E. Strongly interacting array of quantum oscillators coupled to a common cavity field

As a final example, we compute the dynamics of a circular array of quantum harmonic oscillators of size N with periodic boundary conditions. The array oscillator couples strongly to a common cavity field. We monitor the population transfer dynamics between oscillators in the array with the MC-MCTDH method assuming strong bilinear coupling between sites. The effective Hamiltonian is given by

$$\hat{H} = \omega_c\hat{a}^\dagger\hat{a} - \frac{i\kappa}{2}\hat{a}^\dagger\hat{a} + \sum_{i=1}^{N}\left[\omega_0\hat{b}_i^\dagger\hat{b}_i + g(\hat{b}_i^\dagger\hat{a} + \hat{b}_i\hat{a}^\dagger) - \frac{i\gamma}{2}\hat{b}_i^\dagger\hat{b}_i\right]$$
$$+ \sum_{i=1}^{N-1}\lambda(\hat{b}_i^\dagger\hat{b}_{i+1} + \hat{b}_i\hat{b}_{i+1}^\dagger) + \lambda(\hat{b}_1^\dagger\hat{b}_N + \hat{b}_1\hat{b}_N^\dagger), \quad (21)$$

where λ is the nearest-neighbor coupling and the other variables are defined as before.
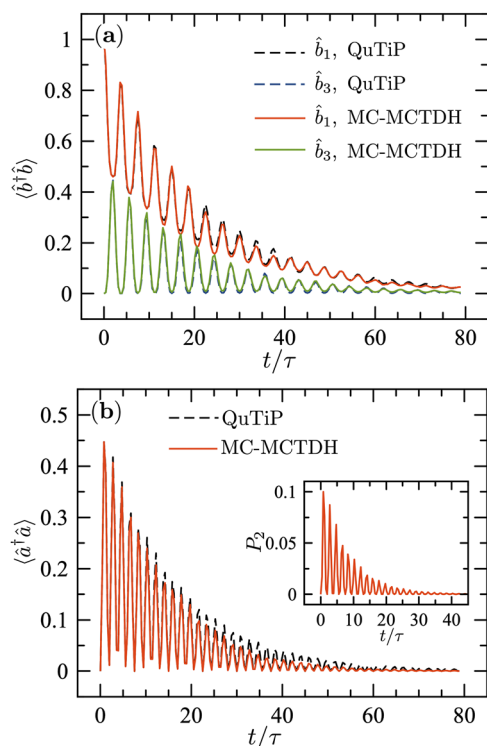
FIG. 5. Cavity-mediated population transfer between N uncoupled oscillators. (a) MC-MCTDH energy transfer between subsystems (b_1, b_3) in a set of $N = 4$ oscillators coupled resonantly with a cavity field, with $n_T = 200$ quantum trajectories (solid lines). (b) Photon occupation number $\langle \hat{a}^\dagger \hat{a} \rangle$ of cavity field using the MC-MCTDH (solid red line) and solving the Lindblad master equation (black dashed line). Inset: Time-dependent projection over Fock state with $n = 2$. The frequencies of the b-oscillators are ω_0, the dissipation rates are $\kappa = 0.026\omega_0$ and $\gamma = 0.013\omega_0$, and the bilinear coupling strength is $g = 0.13\omega_0$. Time in units of $\tau = 2\pi/\omega_0$.

FIG. 6. Population transfer for a strongly coupled oscillator array in a cavity. (a) MC-MCTDH evolution of the cavity occupation number $\langle \hat{a}^\dagger \hat{a} \rangle$ for an array of $N = 4$ oscillators initially in the ground state inside a cavity with $n = 2$ photons (solid red line), for $n_T = 300$ quantum trajectories. The Liouville-space solution (QuTiP) is also shown (dashed black line); (b) the same as panel (a) for two initial array excitations and two cavity photons. The density matrix solution was obtained with an HCP workstation. In both panels, the inset shows the evolution of the occupation number for oscillator b_1. The b-oscillator frequencies are ω_0, the dissipation rates are $\kappa = 0.026\omega_0$ and $\gamma = 0.013\omega_0$, the light–matter coupling strength is $g = 0.13\omega_0$, and the nearest-neighbor coupling in the array is $\lambda = g/2$. Time is in units of $\tau = 2\pi/\omega_0$.

In Fig. 6, we show the occupation numbers of the cavity field and the oscillator $\hat{b}_1$, for an array of size $N = 4$ and an initially excited cavity with $n = 2$ photons. Two array excitation levels are studied. In Fig. 6(a), the oscillator array is set to the ground state ($\nu_{max} = 0$). In this case, the initial cavity excitations are transferred rapidly to the oscillator array creating a many-particle wave packet that eventually decays within a few vibrational lifetimes. The evolution can be converged in Liouville space with a truncated Hilbert space that includes up to $\nu_{max} = 3$ excitations per site and $n_{max} = 5$ photons, giving the Hilbert space dimension $d = 1536$. The converged MC-MCTDH calculations involved $N_k = 41$ grid points for each degree of freedom in a harmonic oscillator-DVR primitive basis, with $n_k = 4$ time-dependent functions, giving 1844 equations of motion to solve. Figure 6(a) shows that the MC-MCTDH expectation values agree with the converged Liouville-space results within ~1% with only $n_T = 300$ quantum trajectories.

In Fig. 6(b), we informally probe the efficiency of the MC-MCTDH method by increasing the initial excitation density of the array to two excitations: one excitation in oscillator b_1 and another excitation in oscillator b_2, again with two initial cavity photons, i.e., $|\Psi(0)\rangle = |1, 1, 0, 0, n = 2\rangle$. For the same Hamiltonian and
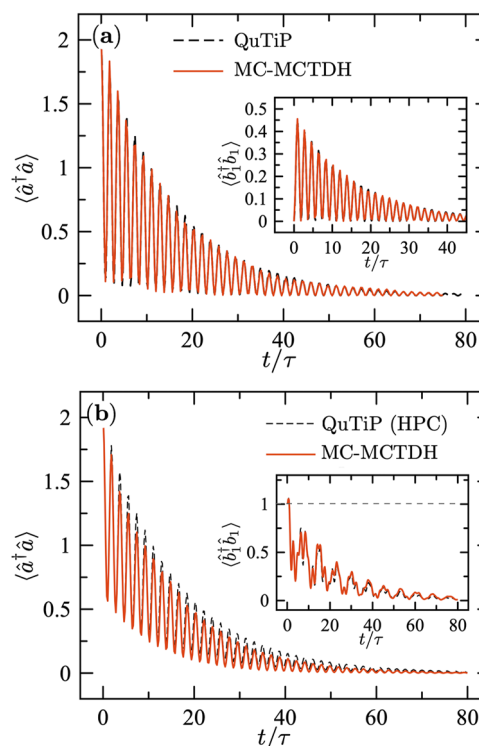
dissipative parameters in Fig. 6(a), convergence of the Liouville space solution was not possible on the same machine where the MC-MCTDH was implemented, due to RAM constraints. We obtained converged density matrix solutions with QuTiP implemented in a high-performance computing (HCP) workstation. The minimum Hilbert space dimension needed for 1% convergence was found to be $d = 10\,368$, which included $\nu_{max} = 5$ excitations per site and $n_{max} = 7$ cavity Fock states. Figure 6(b) shows that the MC-MCTDH solution obtained in the low-RAM machine agrees well with the numerically exact Liouville space solutions for $\hat{a}$ and $\hat{b}$ oscillators in the HCP workstation, using only 300 quantum trajectories.

IV. CONCLUSIONS AND DISCUSSION

Motivated by the current problems in molecular quantum electrodynamics,[9,33,34] we developed an efficient numerical methodology for computing the open system dynamics of strongly coupled quantized oscillators. The method combines the deterministic non-unitary propagation of the many-particle system wave function in

a coordinate space with a sequence of stochastic quantum jumps that model the interaction of the system with multiple reservoirs. The stochastic component of the propagator is based on the Monte Carlo wave function method developed in quantum optics,[14] which, by construction, converges to Lindblad semi-group dynamics.[14] The deterministic steps are implemented using the multi-configuration time-dependent Hartree (MCTDH[46]) method, which was originally developed to describe wave packets with continuous-variable degrees of freedom that are relevant in chemical dynamics.

We demonstrate the applicability of the method by solving the open quantum system dynamics of selected scenarios of current interest: (i) decay dynamics of a lossy optical cavity; (ii) vacuum Rabi oscillations for strongly interacting cavity-vibration systems with photonic and material losses; (iii) population revivals for a two-level system in a driven cavity; (iv) photon-mediated population transfer between independent molecular vibrations coupled to a common cavity field; and (v) quench dynamics in an array of strongly interacting vibrational oscillators with high initial excitation density. In all cases, the proposed method converges to the exact Liouville-space solution with a reasonably low number of quantum trajectories. For an array of strongly coupled oscillators with high excitation density, preliminary tests suggest that the method is more efficient than the currently available open-source quantum optics libraries[67] at equal machine resources.

Applications of this quantum dynamics methodology include the study of vibrational relaxation and rotational depolarization of molecular ensembles in liquid-phase infrared cavities under vibrational strong coupling,[35] which are believed to determine the dynamics of unconventional light–matter coherences that emerge in two-dimensional infrared cavity spectroscopy,[72] and the reactive dynamics of polar molecules under vibrational ultrastrong coupling.[73,74] The methodology can also be implemented with time-dependent Hamiltonians to study coherent control scenarios in nanophotonics.[75–77] Future extensions of the method can be implemented to describe systems with non-Markovian coupling to multiple reservoirs.[49]

ACKNOWLEDGMENTS

AUTHOR DECLARATIONS

Conflict of Interest

The authors have no conflicts to disclose.

Author Contributions

Johan F. Triana: Conceptualization (supporting); Data curation (lead); Formal analysis (lead); Investigation (lead); Methodology (equal); Validation (lead); Visualization (lead); Writing – original draft (lead); Writing – review & editing (supporting). **Felipe Herrera**: Conceptualization (lead); Formal analysis (equal); Funding acquisition (lead); Investigation (supporting); Methodology (equal); Project administration (equal); Resources (lead); Supervision (lead); Validation (equal); Visualization (supporting); Writing – original draft (supporting); Writing – review & editing (lead).

DATA AVAILABILITY

The data that support the findings of this study are available from the corresponding author upon reasonable request.

APPENDIX: EQUIVALENCE OF THE MONTE CARLO WAVE FUNCTION METHOD AND LINDBLAD QUANTUM MASTER EQUATIONS

The time evolution of wave function $|\Psi(t)\rangle$ inside MCWF is performed by finding the wave function at a time $t + \Delta t$ for small enough Δt. At first-order approximation, we obtain (in atomic units)

$$|\Psi(t + \Delta t)^N\rangle = (1 - i\hat{H}\Delta t)|\Psi(t)\rangle, \tag{A1}$$

where $\hat{H}$ is non-Hermitian, $|\Psi(t + \Delta t)^N\rangle$ is not normalized, and hence,

$$\langle\Psi(t + \Delta t)^N|\Psi(t + \Delta t)^N\rangle = 1 - \delta p, \tag{A2}$$

with

$$\delta p = \sum_n \delta p_n = \Delta t \sum_n \langle\Psi(t)|\hat{L}_n^\dagger \hat{L}_n|\Psi(t)\rangle, \tag{A3}$$

where δp_n describes the loss of the norm of jump operator $\hat{L}_n$.

Considering the operator $\hat{\sigma}(t) = |\Psi(t)\rangle\langle\Psi(t)|$, for a defined number of realizations with different random numbers ϵ at time $t + \Delta t$, the average value of $\hat{\sigma}(t + \Delta t)$ is given by

$$\overline{\hat{\sigma}(t + \Delta t)} = (1 - \delta p)|\Psi(t + \Delta t)\rangle\langle\Psi(t + \Delta t)| + \delta p \sum_n \alpha_n |\Psi(t + \Delta t)\rangle\langle\Psi(t + \Delta t)|, \tag{A4}$$

with $\alpha_n = \delta p_n/\delta p$. Inserting Eqs. (4) and (A1) into Eq. (A4), we obtain

$$\overline{\hat{\sigma}(t + \Delta t)} = (1 - i\Delta t\hat{H})\hat{\sigma}(t)(1 + i\Delta t\hat{H}^\dagger) + \delta p \sum_n \alpha_n \frac{\hat{L}_n \hat{\sigma}(t) \hat{L}_n^\dagger}{\delta p_n/\delta t}, \tag{A5}$$

$$\overline{\hat{\sigma}(t + \Delta t)} = \hat{\sigma}(t) - i\Delta t\hat{H}\hat{\sigma}(t) + i\Delta t\hat{\sigma}(t)\hat{H}^\dagger + \Delta t \sum_n \hat{L}_n \hat{\sigma}(t) \hat{L}_n^\dagger + \mathcal{O}(\Delta t^2), \tag{A6}$$

and considering that $\hat{H}$ is given by Eq. (2), we obtain

$$\overline{\hat{\sigma}(t + \Delta t)} = \hat{\sigma}(t) + i\Delta t[\hat{\sigma}(t), \hat{H}_S] - \frac{\Delta t}{2} \sum_n \{\hat{\sigma}(t), \hat{L}_n^\dagger \hat{L}_n\} + \Delta t \sum_n \hat{L}_n \hat{\sigma}(t) \hat{L}_n^\dagger + \mathcal{O}(\Delta t^2). \tag{A7}$$

Now, if we apply the limit $\Delta t \to 0$, Eq. (A7) reduces to

$$\frac{d\overline{\hat{\sigma}}}{dt} = i[\overline{\hat{\sigma}}, \hat{H}_S] + \mathcal{L}[\overline{\hat{\sigma}}], \tag{A8}$$

where $\mathcal{L}[\bar{\hat{\sigma}}]$ is the Lindblad superoperator given by

$$\mathcal{L}[\bar{\hat{\sigma}}] = \sum_n \hat{L}_n \hat{\sigma}(t) \hat{L}_n^\dagger - \frac{1}{2} \sum_n \{\hat{\sigma}(t), \hat{L}_n^\dagger \hat{L}_n\}. \qquad (A9)$$

Note that Eq. (A8) is equivalent to Eq. (1). Hence, we demonstrate the validity of MCWF with the master equation in Lindblad form.

Now, the next step is to calculate the expectation value of a given operator $\hat{O}$, which, according to the density operator in the limits $\Delta t \to 0$ and $n_T \to \infty$, is equivalent to $\langle \hat{O} \rangle = \text{Tr}[\hat{\rho}_S(t)\hat{O}]$. In the MCWF method, the expectation value is calculated by implementing Eq. (6). However, in MCWF, there are numerical errors for a finite number of trajectories n_T. We measure the error by calculating the mean squared error at time t given by

$$\text{MSE}[\overline{\langle \hat{O}(t) \rangle}] = \frac{1}{n_T} \sum_{k=1}^{n_T} \left[\langle \hat{O}(t) \rangle_{(k)} - \langle \hat{O}(t) \rangle \right]^2, \qquad (A10)$$

where $\langle \hat{O}(t) \rangle_{(k)}$ is the expectation value of trajectory k and $\langle \hat{O}(t) \rangle = \text{Tr}[\hat{\rho}_S(t)\hat{O}]$ is the exact solution.

REFERENCES

[1] C. P. Koch, J. Phys.: Condens. Matter **28**, 213001 (2016).

[2] S. Deffner and E. Lutz, Phys. Rev. Lett. **111**, 010402 (2013).

[3] A. W. Chin, S. F. Huelga, and M. B. Plenio, Phys. Rev. Lett. **109**, 233601 (2012).

[4] J. F. Haase, A. Smirne, S. F. Huelga, J. Kołodynski, and R. Demkowicz-Dobrzanski, Quantum Meas. Quantum Metrol. **5**, 13 (2016).

[5] A. Di Paolo, T. E. Baker, A. Foley, D. Sénéchal, and A. Blais, npj Quantum Inf. **7**, 11 (2021).

[6] M. S. Tame, K. R. McEnery, Ş. K. Özdemir, J. Lee, S. A. Maier, and M. S. Kim, Nat. Phys. **9**, 329 (2013).

[7] M. K. Schmidt, R. Esteban, A. González-Tudela, G. Giedke, and J. Aizpurua, ACS Nano **10**, 6291 (2016).

[8] F. Herrera and F. C. Spano, Phys. Rev. Lett. **116**, 238301 (2016).

[9] F. Herrera and J. Owrutsky, J. Chem. Phys. **152**, 100902 (2020).

[10] H. Breuer, P. Breuer, F. Petruccione, and S. Petruccione, *The Theory of Open Quantum Systems* (Oxford University Press, 2002).

[11] D. Manzano, AIP Adv. **10**, 025106 (2020).

[12] H. Weimer, A. Kshetrimayum, and R. Orús, Rev. Mod. Phys. **93**, 015008 (2021).

[13] N. Gisin and I. C. Percival, J. Phys. A: Math. Gen. **25**, 5677 (1992).

[14] J. Dalibard, Y. Castin, and K. Mølmer, Phys. Rev. Lett **68**, 580 (1992); Y. Castin and J. Dalibard, J. Opt. Soc. Am. B **524**, 10 (1993).

[15] E. R. Koessler, A. Mandal, and P. Huo, J. Chem. Phys. **157**, 064101 (2022).

[16] F. Verstraete, J. J. García-Ripoll, and J. I. Cirac, Phys. Rev. Lett. **93**, 207204 (2004).

[17] A. H. Werner, D. Jaschke, P. Silvi, M. Kliesch, T. Calarco, J. Eisert, and S. Montangero, Phys. Rev. Lett. **116**, 237201 (2016).

[18] R. Orús, Nat. Rev. Phys. **1**, 538 (2019).

[19] I. Carusotto and C. Ciuti, Phys. Rev. B **72**, 125335 (2005).

[20] P. Navez and R. Schützhold, Phys. Rev. A **82**, 063603 (2010).

[21] J. Schachenmayer, A. Pikovski, and A. M. Rey, Phys. Rev. X **5**, 011022 (2015).

[22] H. Weimer, Phys. Rev. Lett. **114**, 040402 (2015).

[23] J. Cao and B. J. Berne, J. Chem. Phys. **92**, 7531 (1990).

[24] Y. Tanimura, J. Chem. Phys. **153**, 020901 (2020).

[25] B. Tang, E. Khatami, and M. Rigol, Comput. Phys. Commun. **184**, 557 (2013).

[26] J. Cao and G. A. Voth, J. Chem. Phys. **100**, 5093 (1994).

[27] J. Cao and G. A. Voth, J. Chem. Phys. **100**, 5106 (1994).

[28] L. M. Sieberer, M. Buchhold, and S. Diehl, Rep. Prog. Phys. **79**, 096001 (2016).

[29] S. Valleau, S. K. Saikin, M.-H. Yung, and A. A. Guzik, J. Chem. Phys. **137**, 034109 (2012).

[30] J. M. Moix and J. Cao, J. Chem. Phys. **139**, 134106 (2013).

[31] J. del Pino, F. A. Y. N. Schröder, A. W. Chin, J. Feist, and F. J. Garcia-Vidal, Phys. Rev. Lett. **121**, 227401 (2018).

[32] Y.-S. Wang, P. Nijjar, X. Zhou, D. I. Bondar, and O. V. Prezhdo, J. Phys. Chem. B **124**, 4326 (2020).

[33] F. J. Garcia-Vidal, C. Ciuti, and T. W. Ebbesen, Science **373**, eabd0336 (2021).

[34] J. Feist, J. Galego, and F. J. Garcia-Vidal, ACS Photonics **5**, 205 (2018).

[35] B. S. Simpkins, A. D. Dunkelberger, and J. C. Owrutsky, J. Phys. Chem. C **125**, 19081 (2021).

[36] J. Fregoni, G. Granucci, M. Persico, and S. Corni, Chem **6**, 250 (2020).

[37] S. Felicetti, J. Fregoni, T. Schnappinger, S. Reiter, R. de Vivie-Riedle, and J. Feist, J. Phys. Chem. Lett. **11**, 8810 (2020).

[38] J. Fregoni, S. Corni, M. Persico, and G. Granucci, J. Comput. Chem. **41**, 2033 (2020).

[39] J. A. Campos-Gonzalez-Angulo, R. F. Ribeiro, and J. Yuen-Zhou, Nat. Commun. **10**, 4685 (2019).

[40] P. Antoniou, F. Suchanek, J. F. Varner, and J. J. Foley, J. Phys. Chem. Lett. **11**, 9063 (2020).

[41] M. Du, L. A. Martínez-Martínez, R. F. Ribeiro, Z. Hu, V. M. Menon, and J. Yuen-Zhou, Chem. Sci. **9**, 6659 (2018).

[42] I. S. Ulusoy and O. Vendrell, J. Chem. Phys. **153**, 044108 (2020).

[43] B. Gu and S. Mukamel, Chem. Sci. **11**, 1290 (2020).

[44] W. Ahn, F. Herrera, and B. Simpkins, "Modification of urethane addition reaction via vibrational strong coupling," ChemRxiv: (2022), https://doi.org/10.26434/chemrxiv-2022-wb6vs.

[45] M. B. Plenio and P. L. Knight, Rev. Mod. Phys. **70**, 101 (1998).

[46] H.-D. Meyer, U. Manthe, and L. S. Cederbaum, Chem. Phys. Lett. **165** 73 (1990); M. Beck, A. Jackle, G. Worth, and H.-D. Meyer, Phys. Rep. **324**, 1 (2000).

[47] G. Worth, M. Beck, A. Jäckle, and H. Meyer, The MCTDH Package, version 8.4, http://mctdh.uni-hd.de, 2007.

[48] I. de Vega and D. Alonso, Rev. Mod. Phys. **89**, 015001 (2017).

[49] J. Piilo, K. Härkönen, S. Maniscalco, and K.-A. Suominen, Phys. Rev. A **79**, 062112 (2009).

[50] D. L. Andrews, G. A. Jones, A. Salam, and R. G. Woolley, J. Chem. Phys. **148**, 040901 (2018).

[51] M. A. D. Taylor, A. Mandal, W. Zhou, and P. Huo, Phys. Rev. Lett. **125**, 123602 (2020).

[52] A. Raab and H.-D. Meyer, Theor. Chem. Acc. **104**, 358 (2000).

[53] M. Nest and H.-D. Meyer, J. Chem. Phys. **119**, 24 (2003).

[54] I. Andrianov and P. Saalfrank, J. Chem. Phys. **124**, 034710 (2006).

[55] O. Vendrell and H.-D. Meyer, J. Chem. Phys. **134**, 044135 (2011).

[56] O. Vendrell, Chem. Phys. **509**, 55 (2018), high-dimensional quantum dynamics (on the occasion of the 70th birthday of Hans-Dieter Meyer).

[57] C. L. Cortes, M. Otten, and S. K. Gray, J. Chem. Phys. **152**, 084105 (2020).

[58] S. Mandal, F. Gatti, O. Bindech, R. Marquardt, and J.-C. Tremblay, J. Chem. Phys. **156**, 094109 (2022).

[59] S. Mandal, F. Gatti, O. Bindech, R. Marquardt, and J. C. Tremblay, J. Chem. Phys. **157**, 144105 (2022).

[60] During peer review, we became aware of Refs. 58 and 59 with an equivalent implementation of the Monte Carlo MCTDH scheme developed in this work, but applied to the coupled dynamics of the internal stretch and the surface–molecule distance in the O2/Pt(111) system coupled to a Markovian bath of electron–hole-pairs.

[61] H. Carmichael, *Statistical Methods in Quantum Optics 1: Master Equations and Fokker–Planck Equations* (Springer Berlin/Heidelberg, 1999); *Statistical Methods in Quantum Optics 2: Non-classical Fields* (Springer Berlin/Heidelberg, 2008).

[62] A. D. McLachlan, Mol. Phys. **8**, 39 (1964).

[63] A. Raab, G. A. Worth, H.-D. Meyer, and L. S. Cederbaum, J. Chem. Phys. **110**, 936 (1999).

[64] H. Meyer, F. Gatti, and G. Worth, *Multidimensional Quantum Dynamics: MCTDH Theory and Applications* (John Wiley & Sons, 2009).

[65] J. Light and T. Carrington, Adv. Chem. Phys. **114**, 263 (2000).

[66] H. Meyer, "Introduction to MCTDH: Lecture notes," https://www.pci.uni-heidelberg.de/cms/mctdh.html (2011).

[67] J. R. Johansson, P. D. Nation, and F. Nori, Comput. Phys. Commun. **183**, 1760 (2012).

[68] J. F. Triana, D. Peláez, and J. L. Sanz-Vicario, J. Phys. Chem. A **122**, 2266 (2018).

[69] B. Zhu, A. M. Rey, and J. Schachenmayer, New J. Phys. **21**, 082001 (2019).

[70] E. T. Jaynes and F. W. Cummings, in *Proceedings of the IEEE* (IEEE, 1963), Vol. 51, p. 89.

[71] C. Gerry and P. Knight, *Introductory Quantum Optics* (Cambridge University Press, Cambridge, 2005).

[72] A. B. Grafton, A. D. Dunkelberger, B. S. Simpkins, J. F. Triana, F. J. Hernández, F. Herrera, and J. C. Owrutsky, Nat. Commun. **12**, 214 (2021).

[73] F. J. Hernández and F. Herrera, J. Chem. Phys. **151**, 144116 (2019).

[74] J. F. Triana, F. J. Hernández, and F. Herrera, J. Chem. Phys. **152**, 234111 (2020).

[75] E. A. Muller, B. Pollard, H. A. Bechtel, R. Adato, D. Etezadi, H. Altug, and M. B. Raschke, ACS Photonics **5**, 3594 (2018).

[76] B. Metzger, E. Muller, J. Nishida, B. Pollard, M. Hentschel, and M. B. Raschke, Phys. Rev. Lett. **123**, 153001 (2019).

[77] J. F. Triana, M. Arias, J. Nishida, E. A. Muller, R. Wilcken, S. C. Johnson, A. Delgado, M. B. Raschke, and F. Herrera, J. Chem. Phys. **156**, 124110 (2022).